Journal of Mathematical Modeling
Vol. 14, No. 2, 2026, pp. 699-722. Research Article

JMM

Dual analysis of myocardial infarction using fractional mathematical modeling and machine learning

Tharmalingam Gunasekar[†‡ *], **Sumaiya Banu S S**[†], **Shyam Sundar Santra**[§ *], **Dumitru Baleanu**[¶,◇]

[†]*Department of Mathematics, Vel Tech Rangarajan Dr. Sagunthala R&D Institute of Science and Technology, Chennai - 600062, Tamil Nadu, India*
[‡]*Department of Mathematics, Srinivas University, Mukka, Mangaluru - 574146, Karnataka, India*
[§]*Department of Mathematics, JIS College of Engineering, Kalyani, West Bengal - 741235, India*
[¶]*Department of Computer Science and Mathematics, Lebanese American University, Beirut - 11022801, Lebanon*
[◇]*Institute of Space Sciences-Subsidiary of INFLR, Magurele - Bucharest, Romania*

Email(s): tguna84@gmail.com, sumaiyabanu279@gmail.com, shyam01.math@gmail.com, dumitru.baleanu@lau.edu.lb

Abstract. This paper presents a novel fractional-order mathematical model of myocardial infarction in women who are users of combined oral contraceptive pill and who also develop comorbidity due to various reasons. The system of equations incorporate Caputo fractional derivative to capture memory effects of the model. Existence and uniqueness of solution of the mathematical model is derived. Numerical simulations were rigorously conducted on the model with varying fractional order namely, 0.3, 0.5 and 0.8 using Euler's method. The numerical results thus obtained are simulated by Adam's method for 200 days period. The output from these simulations form the dataset of the Bayesian regularization neural network with dataset split for training, testing and validating the computational model. Bayesian regularization is incorporated to handle overfitting efficiently. Root Mean Square Errors are computed for all three fractional orders respectively. Regression analysis is conducted which yielded perfect correlation $(R = 1)$ across the all datasets. The combined mathematical and computational analysis form a strong layout in myocardial infarction risk prediction, diagnosis and treatment in young women.

Keywords: Myocardial infarction, fractional mathematical modeling, Caputo derivative, combined oral contraceptive pill, Bayesian regularization neural network.
AMS Subject Classification 2010: 97M40, 68T01, 34A34, 92-10, 34A08.

*Corresponding author
Received: 30 August 2025/ Revised: 06 November 2025/ Accepted: 15 December 2025
DOI: 10.22124/jmm.2025.31534.2837

1 Introduction

Myocardial infarction (MI) is a potentially life-threatening cardiovascular disease brought on by the termination of blood flow to the heart muscle, usually as a result of obstruction of the coronary arteries. It leads to ischemia, irreversible damage to myocardial cells, and, in the most extreme case, death. The MI has classically been associated with older individuals; however, contemporary epidemiological trends reveal an alarming rise in prevalence in young adults and even teenagers, making it an emerging public health problem. The prevailing trend increased understanding of the etiology of MI risk factors in younger populations, particularly in females.

Women are specifically affected by various combinations of hormonal, biological, and social and behavioural factors that affect their cardiovascular health. One major factor is the common use of combined oral contraceptive pills (COCP), which are used not only for contraception but also for the treatment of other gynecologic and endocrine disorders including polycystic ovary syndrome (PCOS), polycystic ovarian disease (PCOD), acne, and menstrual disturbances. While COCPs are extremely beneficial, mounting evidence also suggests that their use-especially in the context of prior cardiovascular risk factors-could be a risk factor for thrombotic complications like MI. Literature has shown that COCPs potentially contribute to hypercoagulability, hypertension, and altering lipid profiles, all of which predispose to MI.

The risk for MI is increased when COCP consumption occurs in association with comorbid factors such as diabetes, hypertension, hypercholesterolemia, or undesirable lifestyle practices like cigarette smoking and alcohol consumption. For example, women with comorbid risk factors bear rare and elevated risk of MI, according to clinical as well as population studies. The relationship between COCP and comorbidities presents a multifaceted variable that requires a systematic approach in modeling and measuring the associated risks.

Agbo et al. [1] presented a mathematical model that analyzed the stability of heart disease dynamics and shed light on which parameters favor the persistence of the disease. Along the same line, Agbo et al. [2] examined heart disease transmission and prevention dynamics with respect to stability at the disease-free equilibrium and conditions for the eradication of the disease in the population. In the same direction, Chen-Charpentier and Kojouharov [3] conducted sensitivity and uncertainty analysis on an MI model that, by pointing out the most sensitive parameters, was reassuring for better calibration.

Several studies have been forwarded with a view to elucidating and simulating MI progression and its risk factors using mathematical models. Early epidemiological evidence for oral contraceptive use with an increased risk of MI in women was presented by Croft and Hannaford [4], based on data from the Royal College of General Practitioners' oral contraception study. Fang et al. [6] performed a bibliometric analysis of MI-related publications with the aim of assessing the trends and gaps in research. Gompel et al. [7], in the WAMIF study, investigated contraception and MI risk related to young women, with accentuation of the impact of additional cardiovascular risk factors.

A hybrid neural ordinary differential equations model of the cardiovascular system that combines mechanistic modeling with machine learning was proposed for improved prediction performance by Grigorian et al. [8]. Hammad et al. [9] proposed a deep neural network for the detection of MI from imbalanced datasets and achieved higher performance in various medical diagnosis tasks. In [10], the authors developed a fractional multi-order mathematical model to simulate and predict the dynamics of the COVID-19 outbreak in Morocco, showing how multi-order derivatives capture the memory and heterogeneous transmission dynamics of this disease. The authors proposed and discussed a fractional order

model to estimate and forecast unreported cases of COVID-19 in Morocco to provide new insights into the hidden dynamics of this epidemic and improve forecasting in [11]. A recent study [12] demonstrated a novel way to analyze dynamics of in-vitro fertilization (IVF) via compartmental modeling and predict IVF treatment success rate by integrating with artificial neural networks.

The role of neural networks and computational intelligence in cardiovascular modeling has been reinforced by foundational works such as Haykin [13], which provides theoretical and practical knowledge on neural networks and learning algorithms. Lidegaard et al. [14] presented a large-scale population study linking hormonal contraception to increased risks of MI and thrombotic stroke, with risk levels depending on the type and duration of contraceptive use. A new model for HIV/AIDS transmission was formulated in [15], which contains the Caputo–Fabrizio fractional derivative to highlight optimal control strategies for the prevention of disease spread by means of the non-singular kernel effects. The hybrid model presented in the study [16] includes a GA-IPA and a neural network to arrive at accurate numerical solutions for the given class of fractional-order nonlinear predator–prey systems with better convergence and computational efficiency. The important computational enhancement for the solution in spectral methods has been presented for fractional-order differential equations, showing improved precision and reduced numerical error in [17].

Pedersen et al. [18] reviewed the MI risk factors in both men and women, pointing out sex-specific differences in prevalence and clinical presentation. The authors of [19] have presented new generalizations of weighted nonsingular fractional integral operators, which extend the analytical framework for modeling systems having memory and hereditary properties. Samko et al. [20] presented a complete theoretical framework of fractional integrals and derivatives, including those found in biological systems with memory effects. Serikkalievna et al. [21] discussed the current concept of MI among young people in terms of its etiology and prevention measures. In [22], the authors have investigated the SEITR tuberculosis transmission model using the Caputo–Fabrizio fractional derivative. It has been indicated how the dynamics of long-term TB spread can be affected by different contact rates and how it can be controlled. The work in [23] presents a high-accuracy spectral approach to solving Bagley–Torvik equations and verifies the superior numerical accuracy and stability of this new method for fractional-order dynamic problems.

Research has also identified certain risk factors associated with increased susceptibility to MI. Tanis et al. [24] explored the clinical relationship between the use of oral contraceptives and MI risk, considering hormonal dose and formulation. Tee and Daud [25] proposed a mathematical model to examine population dynamics of heart failure and heart transplantation that provided methods applicable to the modeling of MI. Than et al. [26] used machine learning to determine the likelihood of acute MI and showed the diagnostic potential for AI-driven methods. Vaccarino [27] presented MI as an emerging and undervalued epidemic in young women, including both biological and societal contributors. Yadav et al. [28] introduced neural network methods for solving differential equations, allowing them to be combined with disease modeling. Yonis et al. [29] carried out a nationwide cohort study of stroke and MI risk with contemporary hormonal contraception, providing real-world clinical perspectives. The authors extended the spectral methods by using generalized Laguerre polynomials in [30], which enabled them to solve time fractional Bloch equations and increased the computational efficiency while increasing the accuracy of complex physical systems. This work [31] defined threshold conditions and evaluated the efficiency of various non-pharmaceutical intervention strategies aimed at COVID-19 elimination and, therefore, provided a quantitative framework for epidemic control. The study in [32] discusses about the gender differences in the emergence and clinical perception of acute myocardial infarction, projecting

how men are more prone to get acute MI than women.

In this paper, a novel fractional-order compartmental model is proposed to showcase the dynamics of myocardial infarction in female population, with specific focus on the combined effects of COCP usage and comorbidities such as hypertension, diabetes, hypercholesterolemia, etc. The model incorporates transitions between susceptible, contraceptive use, multi-use, comorbidity, MI, treatment, and recovery compartments. Numerical simulations are conducted under various fractional orders to capture the memory effects inherent in biological processes. The simulated data serve as inputs to a neural network for prediction and error analysis, bridging the gap between theoretical modeling and data-driven forecasting. By combining fractional-order modeling with neural network methodologies, this study aims to provide an improved understanding of MI risk in women, particularly in younger age groups, and inform targeted prevention strategies.

The contents of this paper are structured as follows: Section 1 presents the basics insights on MI, usage of COCP and it's impact on women's health. Also, a brief review on the literature available about MI, the influence of COCP on precursor of MI, fractional calculus analysis and neural network approach on MI with different perspective is also shared in this section. In Section 2, illustrates the mathematical model of MI with detailed description about the diverse compartments and parameters used in the model. In addition, the model's system of equations with respective initial conditions incorporated with the derivative is presented. Section 3 expresses the analytical framework of the system model. Section 4 demonstrate the numerical simulation results. In Section 5, the architecture of the BRNN is provided. Section 6 expresses the results and final outcome of the neural network analysis. Sensitivity analysis of various fractional orders with regard to the model's prediction is presented in Section 7. Conclusion of the paper is discussed in Section 8 followed by relevant referred sources.

Definition 1. *([5]) Let $h(t)$ be an integrable function. The Caputo fractional derivative of order $\alpha \in (0,1)$ is define as*

$$ {}^{C}D_t^{\alpha} h(t) = \frac{1}{\Gamma(m-\alpha)} \int_0^t \frac{h^{(m)}(\vartheta)}{(t-\vartheta)^{\alpha-m+1}} \, d\vartheta, \quad m = [\alpha] + 1 \tag{1} $$

where $[\alpha]$ denotes the integer part of α. The equivalent fractional integral of order α (for $Re(\alpha) > 0$) is given by

$$ {}^{C}I_t^{\alpha} h(t) = \frac{1}{\Gamma(\alpha)} \int_0^t \frac{h(\vartheta)}{(t-\vartheta)^{1-\alpha}} \, d\vartheta. \tag{2} $$

Lemma 1. *([20]) The function $h \in C[0,T]$ is a solution of the following fractional differential equation:*

$$ {}^{C}D_t^{\alpha} h(t) = f(t, h(t)), \; h(0) = h_0, \tag{3} $$

if and only if it is a solution of the nonlinear Volterra integral equation of the second kind

$$ h(t) = h(0) + \frac{1}{\Gamma(\alpha)} \int_0^t (t-\vartheta)^{\alpha-1} f(\vartheta, h(\vartheta)) d\vartheta. \tag{4} $$

2 Mathematical model of myocardial infarction

A compartmental framework (1) consisting of ten compartments namely, susceptible women population (S), women population using COCP for contraception (C_1), women using COCP for both contraceptive

and non-contraceptive benefits (B_1), female using COCP for non - contraceptive needs (N_1), contraception based COCP user who develop comorbidity (C_2), multi-purpose COCP female user who develop co – morbidity (B_2), non-contraceptive purpose COCP user ho develop comorbidity (N_2), women affected with MI (M), women under treatment (T) and women under recovery (R) is constructed (Figure 1).

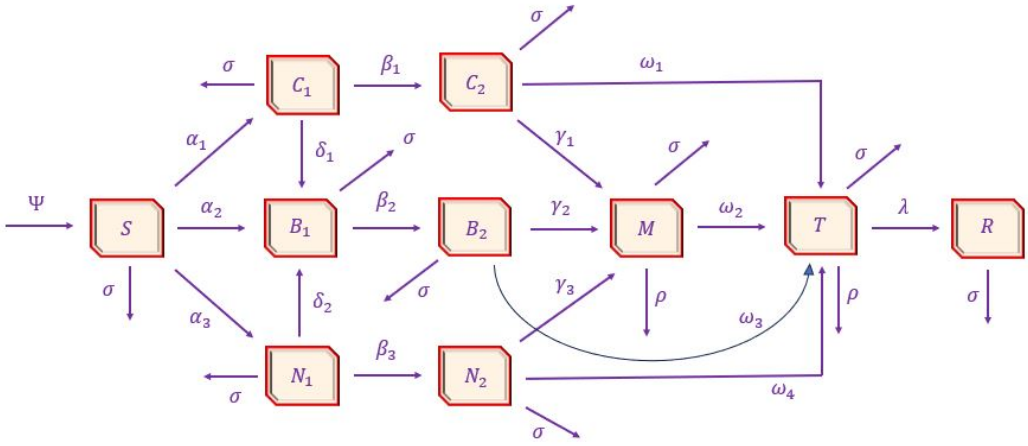

Figure 1: Model depicting the onset of myocardial infarction via COCP and comorbidity influence.

The impact of COCP and other comorbidities in emerging of MI is represented by the system of differential equations as follows:

$$
\begin{aligned}
\frac{dS}{dt} &= \Psi - (\alpha_1+\alpha_2+\alpha_3+\sigma)S,\\
\frac{dC_1}{dt} &= \alpha_1 S - (\beta_1-\delta_1-\sigma)C_1,\\
\frac{dB_1}{dt} &= \alpha_2 S + \delta_1 C_1 + \delta_2 N_1 - (\beta_2+\sigma)B_1,\\
\frac{dN_1}{dt} &= \alpha_3 S - (\delta_2+\beta_3+\sigma)N_1,\\
\frac{dC_2}{dt} &= \beta_1 C_1 - (\gamma_1+\omega_1+\sigma)C_2,\\
\frac{dB_2}{dt} &= \beta_2 B_1 - (\gamma_2+\omega_3+\sigma)B_2,\\
\frac{dN_2}{dt} &= \beta_3 N_1 - (\gamma_3+\omega_4+\sigma)N_2,\\
\frac{dM}{dt} &= \gamma_1 C_2 + \gamma_2 B_2 + \gamma_3 N_2 - (\omega_2+\rho+\sigma)M,\\
\frac{dT}{dt} &= \omega_1 C_2 + \omega_2 M + \omega_3 B_2 + \omega_4 N_2 - (\lambda+\rho+\sigma)T,\\
\frac{dR}{dt} &= \lambda T - \sigma R,
\end{aligned}
\tag{5}
$$

with the initial condition as follows, $S(0) = S_0$, $C_1(0) = C_{10}$, $B_1(0) = B_{10}$, $N_1(0) = N_{10}$, $C_2(0) = C_{20}$, $B_2(0) = B_{20}$, $N_2(0) = N_{20}$ $M(0) = M_0$, $T(0) = T_0$, $R(0) = R_0$.
The transitional parameters utilized in the compartmental model are presented in the Table 1.

Table 1: Model parameters with descriptions

Parameter	Description
Ψ	Rate of inflow of susceptible female population
α_1	Rate of susceptible women who initiate COCP usage for contraception only
α_2	Proportion of female who begin using COCP for both contraception and non-contraception
α_3	Rate of women starting COCP for non-contraceptive reasons
δ_1	Transition rate from contraception to multi-purpose COCP use
δ_2	Change in usage from non-contraceptive to multi-purpose COCP use
β_1	Transition rate of women using COCP for contraception to developing a comorbidity
β_2	Transition rate of women using COCP for multi-purpose to developing a comorbidity
β_3	Transition rate of women using COCP for non-contraception to developing a comorbidity
γ_1	Probability of myocardial infarction in women with comorbidity who use COCP for contraceptive purpose
γ_2	Probability of myocardial infarction in women with comorbidity who use COCP for dual-purpose
γ_3	Probability of myocardial infarction in women with comorbidity who use COCP for non-contraceptive purpose
ω_1	Treatment rate for comorbidity in women who use COCP for contraception
ω_2	Myocardial infarction treatment rate
ω_3	Treatment rate for comorbidity in women who use COCP for dual-purpose
ω_4	Treatment rate for comorbidity in women who use COCP for non-contraception
λ	Recovery rate of women undergoing treatment for myocardial infarction
ρ	Mortality rate due to myocardial infarction
σ	Natural death rate

To emphasize the importance of memory-dependent and non-local behaviors in the system, equations (5) is reformulated using Caputo fractional derivatives. However, this modification introduces dimensional inconsistency between terms. Following the established approaches in fractional modeling, the parameter ζ (with dimensions of seconds) is introduced to maintain dimensional balance across all terms. The fractional order model of COCP and comorbidity induced myocardial infarction for $t > 0$ and $\alpha \in (0,1)$ is given as

$$\begin{aligned} \zeta^{\alpha-1} {}^{C}D_t^{\alpha} S &= \Psi - (\alpha_1 + \alpha_2 + \alpha_3 + \sigma) S, \\ \zeta^{\alpha-1} {}^{C}D_t^{\alpha} C_1 &= \alpha_1 S - (\beta_1 - \delta_1 - \sigma) C_1, \end{aligned} \tag{6}$$

$$
\begin{aligned}
\zeta^{\alpha-1}{}^{C}D_t^{\alpha}B_1 &= \alpha_2 S + \delta_1 C_1 + \delta_2 N_1 - (\beta_2 + \sigma) B_1,\\
\zeta^{\alpha-1}{}^{C}D_t^{\alpha}N_1 &= \alpha_3 S - (\delta_2 + \beta_3 + \sigma) N_1,\\
\zeta^{\alpha-1}{}^{C}D_t^{\alpha}C_2 &= \beta_1 C_1 - (\gamma_1 + \omega_1 + \sigma) C_2,\\
\zeta^{\alpha-1}{}^{C}D_t^{\alpha}B_2 &= \beta_2 B_1 - (\gamma_2 + \omega_3 + \sigma) B_2,\\
\zeta^{\alpha-1}{}^{C}D_t^{\alpha}N_2 &= \beta_3 N_1 - (\gamma_3 + \omega_4 + \sigma) N_2,\\
\zeta^{\alpha-1}{}^{C}D_t^{\alpha}M &= \gamma_1 C_2 + \gamma_2 B_2 + \gamma_3 N_2 - (\omega_2 + \rho + \sigma) M,\\
\zeta^{\alpha-1}{}^{C}D_t^{\alpha}T &= \omega_1 C_2 + \omega_2 M + \omega_3 B_2 + \omega_4 N_2 - (\lambda + \rho + \sigma) T,\\
\zeta^{\alpha-1}{}^{C}D_t^{\alpha}R &= \lambda T - \sigma R,
\end{aligned}
$$

with the initial condition as follows, $S(0) = S_0$, $C_1(0) = C_{10}$, $B_1(0) = B_{10}$, $N_1(0) = N_{10}$, $C_2(0) = C_{20}$, $B_2(0) = B_{20}$, $N_2(0) = N_{20}$ $M(0) = M_0$, $T(0) = T_0$, $R(0) = R_0$.

3 Existence and uniqueness results

The focus of this section is to explore the existence and uniqueness of the proposed model by using the the concept of fixed point theory. Firstly, we proceed by showing that the system exhibits a unique solution. We write the system of equations (6) as follows:

$$
\begin{aligned}
\zeta^{\alpha-1}{}^{C}D_t^{\alpha}S(t) &= X_1(t, S(t)),\\
\zeta^{\alpha-1}{}^{C}D_t^{\alpha}C_1(t) &= X_2(t, C_1(t)),\\
\zeta^{\alpha-1}{}^{C}D_t^{\alpha}B_1(t) &= X_3(t, B_1(t)),\\
\zeta^{\alpha-1}{}^{C}D_t^{\alpha}N_1(t) &= X_4(t, N_1(t)),\\
\zeta^{\alpha-1}{}^{C}D_t^{\alpha}C_2(t) &= X_5(t, C_2(t)),\\
\zeta^{\alpha-1}{}^{C}D_t^{\alpha}B_2(t) &= X_6(t, B_2(t)),\\
\zeta^{\alpha-1}{}^{C}D_t^{\alpha}N_2(t) &= X_7(t, N_2(t)),\\
\zeta^{\alpha-1}{}^{C}D_t^{\alpha}M(t) &= X_8(t, M(t)),\\
\zeta^{\alpha-1}{}^{C}D_t^{\alpha}T(t) &= X_9(t, T(t)),\\
\zeta^{\alpha-1}{}^{C}D_t^{\alpha}R(t) &= X_{10}(t, R(t)),
\end{aligned}
\tag{7}
$$

where

$$
\begin{aligned}
X_1(t, S(t)) &= \Psi - (\alpha_1 + \alpha_2 + \alpha_3 + \sigma) S,\\
X_2(t, C_1(t)) &= \alpha_1 S - (\beta_1 - \delta_1 - \sigma) C_1,\\
X_3(t, B_1(t)) &= \alpha_2 S + \delta_1 C_1 + \delta_2 N_1 - (\beta_2 + \sigma) B_1,\\
X_4(t, N_1(t)) &= \alpha_3 S - (\delta_2 + \beta_3 + \sigma) N_1,\\
X_5(t, C_2(t)) &= \beta_1 C_1 - (\gamma_1 + \omega_1 + \sigma) C_2,\\
X_6(t, B_2(t)) &= \beta_2 B_1 - (\gamma_2 + \omega_3 + \sigma) B_2,\\
X_7(t, N_2(t)) &= \beta_3 N_1 - (\gamma_3 + \omega_4 + \sigma) N_2,
\end{aligned}
$$

$$X_8(t,M(t)) = \gamma_1 C_2 + \gamma_2 B_2 + \gamma_3 N_2 - (\omega_2 + \rho + \sigma) M,$$
$$X_9(t,T(t)) = \omega_1 C_2 + \omega_2 M + \omega_3 B_2 + \omega_4 N_2 - (\lambda + \rho + \sigma) T,$$
$$X_{10}(t,R(t)) = \lambda T - \sigma R.$$

Consider $S(t), C_1(t), B_1(t), N_1(t), C_2(t), B_2(t), N_2(t), M(T), T(t)$ and $R(t)$ are positive bounded functions, which applies that there exists some non-negative constants Ξ_1, Ξ_2, Ξ_3, Ξ_4, Ξ_5, Ξ_6, Ξ_7, Ξ_8, Ξ_9, Ξ_{10} such that
$\|S(t)\| \leq \Xi_1$, $\|C_1(t)\| \leq \Xi_2$, $\|B_1(t)\| \leq \Xi_3$, $\|N_1(t)\| \leq \Xi_4$, $\|C_2(t)\| \leq \Xi_5$, $\|B_2(t)\| \leq \Xi_6$, $\|N_2(t)\| \leq \Xi_7$, $\|M(t)\| \leq \Xi_8$, $\|T(t)\| \leq \Xi_9$, $\|R(t)\| \leq \Xi_{10}$.

In the following theorem, it is demonstrated that the kernels X_i where $i = 1,2,...,10$ satisfy Lipschitz condition and contraction property.

Theorem 1. *Let X_i for $i = 1,2,\cdots,10$ be the kernel function of the system. They satisfy Lipschitz condition and contraction principle, if the following condition holds:*

$$0 \leq K = max\{\Upsilon_1, \Upsilon_2, \Upsilon_3, \Upsilon_4, \Upsilon_5, \Upsilon_6, \Upsilon_7, \Upsilon_8, \Upsilon_9, \Upsilon_{10}\} < 1.$$

Proof. First we consider the function X_1. For any S and S^* we have

$$\begin{aligned} ||X_1(t,S) - X_1(t,S^*)|| &= ||-(\alpha_1 + \alpha_2 + \alpha_3 + \sigma)(S(t) - S^*(t))|| \\ &\leq (\alpha_1 + \alpha_2 + \alpha_3 + \sigma)||(S(t) - S^*(t))|| \\ &\leq \Upsilon_1 ||(S(t) - S^*(t))||, \end{aligned}$$

where $\Upsilon_1 = \alpha_1 + \alpha_2 + \alpha_3 + \sigma$. Thus X_1 satisfy Lipschitz condition.
Similarly, the Lipschitz condition for $X_i = 2,3,\cdots,10$ is given as follows:

$$\begin{aligned} &||X_2(t,C_1) - X_2(t,C_1^*)|| \leq \Upsilon_2 ||C_1(t) - C_1^*(t)||, \\ &||X_3(t,B_1) - X_3(t,B_1^*)|| \leq \Upsilon_3 ||B_1(t) - B_1^*(t)||, \\ &||X_4(t,N_1) - X_4(t,N_1^*)|| \leq \Upsilon_4 ||N_1(t) - N_1^*(t)||, \\ &||X_5(t,C_2) - X_5(t,C_2^*)|| \leq \Upsilon_5 ||C_2(t) - C_2^*(t)||, \\ &||X_6(t,B_2) - X_6(t,B_2^*)|| \leq \Upsilon_6 ||B_2(t) - B_2^*(t)||, \\ &||X_7(t,N_2) - X_7(t,N_2^*)|| \leq \Upsilon_7 ||N_2(t) - N_2^*(t)||, \\ &||X_8(t,M) - X_8(t,M^*)|| \leq \Upsilon_8 ||M(t) - M^*(t)||, \\ &||X_9(t,T) - X_9(t,T^*)|| \leq \Upsilon_9 ||T(t) - T^*(t)||, \\ &||X_{10}(t,R) - X_{10}(t,R^*)|| \leq \Upsilon_{10} ||R(t) - R^*(t)||. \end{aligned}$$

Thus Lipschitz condition is satisfied.
Moreover, under the condition $0 \leq K = max\{\Upsilon_1, \Upsilon_2, \Upsilon_3, \Upsilon_4, \Upsilon_5, \Upsilon_6, \Upsilon_7, \Upsilon_8, \Upsilon_9, \Upsilon_{10}\} < 1$, the kernel functions are contraction mappings. □

By using Lemma 1, the above set of equations (7) can be rewritten as follows:

$$\begin{aligned}
S(t) &= S(0) + \frac{\zeta^{1-\alpha}}{\Gamma(\alpha)} \int_0^t (t-\vartheta)^{\alpha-1} X_1(\vartheta, S(\vartheta)) d\vartheta, \\
C_1(t) &= C_1(0) + \frac{\zeta^{1-\alpha}}{\Gamma(\alpha)} \int_0^t (t-\vartheta)^{\alpha-1} X_2(\vartheta, C_1(\vartheta)) d\vartheta, \\
B_1(t) &= B_1(0) + \frac{\zeta^{1-\alpha}}{\Gamma(\alpha)} \int_0^t (t-\vartheta)^{\alpha-1} X_3(\vartheta, B_1(\vartheta)) d\vartheta, \\
N_1(t) &= N_1(0) + \frac{\zeta^{1-\alpha}}{\Gamma(\alpha)} \int_0^t (t-\vartheta)^{\alpha-1} X_4(\vartheta, N_1(\vartheta)) d\vartheta, \\
C_2(t) &= C_2(0) + \frac{\zeta^{1-\alpha}}{\Gamma(\alpha)} \int_0^t (t-\vartheta)^{\alpha-1} X_5(\vartheta, C_2(\vartheta)) d\vartheta, \\
B_2(t) &= B_2(0) + \frac{\zeta^{1-\alpha}}{\Gamma(\alpha)} \int_0^t (t-\vartheta)^{\alpha-1} X_6(\vartheta, B_2(\vartheta)) d\vartheta, \\
N_2(t) &= N_2(0) + \frac{\zeta^{1-\alpha}}{\Gamma(\alpha)} \int_0^t (t-\vartheta)^{\alpha-1} X_7(\vartheta, N_2(\vartheta)) d\vartheta, \\
M(t) &= M(0) + \frac{\zeta^{1-\alpha}}{\Gamma(\alpha)} \int_0^t (t-\vartheta)^{\alpha-1} X_8(\vartheta, M(\vartheta)) d\vartheta, \\
T(t) &= T(0) + \frac{\zeta^{1-\alpha}}{\Gamma(\alpha)} \int_0^t (t-\vartheta)^{\alpha-1} X_9(\vartheta, T(\vartheta)) d\vartheta, \\
R(t) &= R(0) + \frac{\zeta^{1-\alpha}}{\Gamma(\alpha)} \int_0^t (t-\vartheta)^{\alpha-1} X_{10}(\vartheta, R(\vartheta)) d\vartheta.
\end{aligned} \tag{8}$$

To satisfy the condition that the system has at least one solution, we require the following recursive technique.
Rewrite (7) recursively as follows:

$$\begin{aligned}
S_n(t) &= \frac{\zeta^{1-\alpha}}{\Gamma(\alpha)} \int_0^t (t-\vartheta)^{\alpha-1} X_1(\vartheta, S_{n-1}) d\vartheta, \\
C_{1n}(t) &= \frac{\zeta^{1-\alpha}}{\Gamma(\alpha)} \int_0^t (t-\vartheta)^{\alpha-1} X_2(\vartheta, C_{1n-1}) d\vartheta, \\
B_{1n}(t) &= \frac{\zeta^{1-\alpha}}{\Gamma(\alpha)} \int_0^t (t-\vartheta)^{\alpha-1} X_3(\vartheta, B_{1n-1}) d\vartheta, \\
N_{1n}(t) &= \frac{\zeta^{1-\alpha}}{\Gamma(\alpha)} \int_0^t (t-\vartheta)^{\alpha-1} X_4(\vartheta, N_{1n-1}) d\vartheta, \\
C_{2n}(t) &= \frac{\zeta^{1-\alpha}}{\Gamma(\alpha)} \int_0^t (t-\vartheta)^{\alpha-1} X_5(\vartheta, C_{2n-1}) d\vartheta, \\
B_{2n}(t) &= \frac{\zeta^{1-\alpha}}{\Gamma(\alpha)} \int_0^t (t-\vartheta)^{\alpha-1} X_6(\vartheta, B_{2n-1}) d\vartheta, \\
N_{2n}(t) &= \frac{\zeta^{1-\alpha}}{\Gamma(\alpha)} \int_0^t (t-\vartheta)^{\alpha-1} X_7(\vartheta, N_{2n-1}) d\vartheta,
\end{aligned}$$

$$M_n(t) = \frac{\zeta^{1-\alpha}}{\Gamma(\alpha)} \int_0^t (t-\vartheta)^{\alpha-1} X_8(\vartheta, M_{n-1}) d\vartheta,$$
$$T_n(t) = \frac{\zeta^{1-\alpha}}{\Gamma(\alpha)} \int_0^t (t-\vartheta)^{\alpha-1} X_9(\vartheta, T_{n-1}) d\vartheta,$$
$$R_n(t) = \frac{\zeta^{1-\alpha}}{\Gamma(\alpha)} \int_0^t (t-\vartheta)^{\alpha-1} X_{10}(\vartheta, R_{n-1}) d\vartheta.$$

By taking the initial conditions in consideration and by rewriting the above recursively formed system of equations, we construct the following equations:

$$A_{1n}(t) = S_n(t) - S_{n-1}(t) = \frac{\zeta^{1-\alpha}}{\Gamma(\alpha)} \int_0^t (X_1(\vartheta, S_{n-1}) - X_1(\vartheta, S_{n-2}))(t-\vartheta)^{\alpha-1} d\vartheta,$$
$$A_{2n}(t) = C_{1n}(t) - C_{1n-1}(t) = \frac{\zeta^{1-\alpha}}{\Gamma(\alpha)} \int_0^t (X_2(\vartheta, C_{1n-1}) - X_2(\vartheta, C_{1n-2}))(t-\vartheta)^{\alpha-1} d\vartheta,$$
$$A_{3n}(t) = B_{1n}(t) - B_{1n-1}(t) = \frac{\zeta^{1-\alpha}}{\Gamma(\alpha)} \int_0^t (X_3(\vartheta, B_{1n-1}) - X_3(\vartheta, B_{1n-2}))(t-\vartheta)^{\alpha-1} d\vartheta,$$
$$A_{4n}(t) = N_{1n}(t) - N_{1n-1}(t) = \frac{\zeta^{1-\alpha}}{\Gamma(\alpha)} \int_0^t (X_4(\vartheta, N_{1n-1}) - X_4(\vartheta, N_{1n-2}))(t-\vartheta)^{\alpha-1} d\vartheta,$$
$$A_{5n}(t) = C_{2n}(t) - C_{2n-1}(t) = \frac{\zeta^{1-\alpha}}{\Gamma(\alpha)} \int_0^t (X_5(\vartheta, C_{2n-1}) - X_5(\vartheta, C_{2n-2}))(t-\vartheta)^{\alpha-1} d\vartheta,$$
$$A_{6n}(t) = B_{2n}(t) - B_{2n-1}(t) = \frac{\zeta^{1-\alpha}}{\Gamma(\alpha)} \int_0^t (X_6(\vartheta, B_{2n-1}) - X_6(\vartheta, B_{2n-2}))(t-\vartheta)^{\alpha-1} d\vartheta,$$
$$A_{7n}(t) = N_{2n}(t) - N_{2n-1}(t) = \frac{\zeta^{1-\alpha}}{\Gamma(\alpha)} \int_0^t (X_7(\vartheta, N_{2n-1}) - X_7(\vartheta, N_{2n-2}))(t-\vartheta)^{\alpha-1} d\vartheta,$$
$$A_{8n}(t) = M_n(t) - M_{n-1}(t) = \frac{\zeta^{1-\alpha}}{\Gamma(\alpha)} \int_0^t (X_8(\vartheta, M_{n-1}) - X_8(\vartheta, M_{n-2}))(t-\vartheta)^{\alpha-1} d\vartheta,$$
$$A_{9n}(t) = T_n(t) - T_{n-1}(t) = \frac{\zeta^{1-\alpha}}{\Gamma(\alpha)} \int_0^t (X_9(\vartheta, T_{n-1}) - X_9(\vartheta, T_{n-2}))(t-\vartheta)^{\alpha-1} d\vartheta,$$
$$A_{10n}(t) = R_n(t) - R_{n-1}(t) = \frac{\zeta^{1-\alpha}}{\Gamma(\alpha)} \int_0^t (X_{10}(\vartheta, R_{n-1}) - X_{10}(\vartheta, R_{n-2}))(t-\vartheta)^{\alpha-1} d\vartheta.$$

Consider

$$\begin{aligned} ||A_{1n}(t)|| &= ||S_n(t) - S_{n-1}(t)|| \\ &= ||\frac{\zeta^{1-\alpha}}{\Gamma(\alpha)} \int_0^t (X_1(\vartheta, S_{n-1}) - X_1(\vartheta, S_{n-2}))(t-\vartheta)^{\alpha-1} d\vartheta|| \\ &\leq \frac{\zeta^{1-\alpha}}{\Gamma(\alpha)} \int_0^t ||(X_1(\vartheta, S_{n-1}) - X_1(\vartheta, S_{n-2}))(t-\vartheta)^{\alpha-1}|| d\vartheta \\ &\leq \frac{\zeta^{1-\alpha}}{\Gamma(\alpha)} \Upsilon_1 \int_0^t ||S_{n-1}(t) - S_{n-2}(t)|| d\vartheta \\ &\leq \frac{\zeta^{1-\alpha}}{\Gamma(\alpha)} \Upsilon_1 \int_0^t ||A_{1(n-1)}(t)|| d\vartheta. \end{aligned} \tag{9}$$

In a similar manner, we exhibit that

$$\begin{aligned}
||A_{2n}(t)|| &\leq \tfrac{\zeta^{1-\alpha}}{\Gamma(\alpha)}\Upsilon_2 \int_0^t ||A_{2(n-1)}(t)||d\vartheta,\\
||A_{3n}(t)|| &\leq \tfrac{\zeta^{1-\alpha}}{\Gamma(\alpha)}\Upsilon_3 \int_0^t ||A_{3(n-1)}(t)||d\vartheta,\\
||A_{4n}(t)|| &\leq \tfrac{\zeta^{1-\alpha}}{\Gamma(\alpha)}\Upsilon_4 \int_0^t ||A_{4(n-1)}(t)||d\vartheta,\\
||A_{5n}(t)|| &\leq \tfrac{\zeta^{1-\alpha}}{\Gamma(\alpha)}\Upsilon_5 \int_0^t ||A_{5(n-1)}(t)||d\vartheta,\\
||A_{6n}(t)|| &\leq \tfrac{\zeta^{1-\alpha}}{\Gamma(\alpha)}\Upsilon_6 \int_0^t ||A_{6(n-1)}(t)||d\vartheta,\\
||A_{7n}(t)|| &\leq \tfrac{\zeta^{1-\alpha}}{\Gamma(\alpha)}\Upsilon_7 \int_0^t ||A_{7(n-1)}(t)||d\vartheta,\\
||A_{8n}(t)|| &\leq \tfrac{\zeta^{1-\alpha}}{\Gamma(\alpha)}\Upsilon_8 \int_0^t ||A_{8(n-1)}(t)||d\vartheta,\\
||A_{9n}(t)|| &\leq \tfrac{\zeta^{1-\alpha}}{\Gamma(\alpha)}\Upsilon_9 \int_0^t ||A_{9(n-1)}(t)||d\vartheta,\\
||A_{10n}(t)|| &\leq \tfrac{\zeta^{1-\alpha}}{\Gamma(\alpha)}\Upsilon_{10} \int_0^t ||A_{10(n-1)}(t)||d\vartheta.
\end{aligned} \tag{10}$$

Thus, we can say that

$$S_n(t)=\sum_{j=1}^{n}A_{1j}(t),\ C_{1n}(t)=\sum_{j=1}^{n}A_{2j}(t),\ B_{1n}(t)=\sum_{j=1}^{n}A_{3j}(t),\ N_{1n}(t)=\sum_{j=1}^{n}A_{4j}(t),\ C_{2n}(t)=\sum_{j=1}^{n}A_{5j}(t),$$
$$B_{2n}(t)=\sum_{j=1}^{n}A_{6j}(t),\ N_{2n}(t)=\sum_{j=1}^{n}A_{7j}(t),\ M_n(t)=\sum_{j=1}^{n}A_{8j}(t),\ T_n(t)=\sum_{j=1}^{n}A_{9j}(t),\ R_n(t)=\sum_{j=1}^{n}A_{10j}(t).$$

Theorem 2. *If there exists $t^*>0$ such that $\frac{\zeta^{1-\alpha}}{\Gamma(\alpha)}t^*\Upsilon_i<1$, for $i=1,2,\cdots,10$, then the system (6) admits at least one solution.*

Proof. Since, the function $S(t),C_1(t),B_1(t),N_1(t),C_2(t),B_2(t),N_2(t),M(t),T(t)$ and $R(t)$ are bounded and each kernel X_i for $i=1,2,\cdots,10$ satisfy the Lipschitz conditions, and by using the recursion technique, from equations (8) and (10), we obtain

$$\begin{aligned}
||A_{1n}(t)|| &\leq ||S_n(0)||[\frac{\zeta^{1-\alpha}}{\Gamma(\alpha)}\Upsilon_1 t]^n,\\
||A_{2n}(t)|| &\leq ||C_{1n}(0)||[\frac{\zeta^{1-\alpha}}{\Gamma(\alpha)}\Upsilon_2 t]^n,\\
||A_{3n}(t)|| &\leq ||B_{1n}(0)||[\frac{\zeta^{1-\alpha}}{\Gamma(\alpha)}\Upsilon_3 t]^n,\\
||A_{4n}(t)|| &\leq ||N_{1n}(0)||[\frac{\zeta^{1-\alpha}}{\Gamma(\alpha)}\Upsilon_4 t]^n,\\
||A_{5n}(t)|| &\leq ||C_{2n}(0)||[\frac{\zeta^{1-\alpha}}{\Gamma(\alpha)}\Upsilon_5 t]^n,
\end{aligned}$$

$$||A_{6n}(t)|| \leq ||B_{2n}(0)||[\frac{\zeta^{1-\alpha}}{\Gamma(\alpha)}\Upsilon_6 t]^n,$$
$$||A_{7n}(t)|| \leq ||N_{2n}(0)||[\frac{\zeta^{1-\alpha}}{\Gamma(\alpha)}\Upsilon_7 t]^n,$$
$$||A_{8n}(t)|| \leq ||M_n(0)||[\frac{\zeta^{1-\alpha}}{\Gamma(\alpha)}\Upsilon_8 t]^n,$$
$$||A_{9n}(t)|| \leq ||T_n(0)||[\frac{\zeta^{1-\alpha}}{\Gamma(\alpha)}\Upsilon_9 t]^n,$$
$$||A_{10n}(t)|| \leq ||R_n(0)||[\frac{\zeta^{1-\alpha}}{\Gamma(\alpha)}\Upsilon_{10} t]^n.$$

Therefore the above system of equations show the existence of solution which is also continuous. We will now demonstrate that the above mentioned functions converge to the system of solutions of (7). After completion of n-iterations, let us define the remainder terms $G_{1n}(t)$, $G_{2n}(t)$, $G_{3n}(t)$, $G_{4n}(t)$, $G_{5n}(t)$, $G_{6n}(t)$, $G_{7n}(t)$, $G_{8n}(t)$, $G_{9n}(t)$ and $G_{10n}(t)$.
Consider

$$S(t) - S(0) = S_n(t) - G_{1n}(t),$$
$$C_1(t) - C_1(0) = C_{1n}(t) - G_{2n}(t),$$
$$B_1(t) - B_1(0) = B_{1n}(t) - G_{3n}(t),$$
$$N_1(t) - N_1(0) = N_{1n}(t) - G_{4n}(t),$$
$$C_2(t) - C_2(0) = C_{2n}(t) - G_{5n}(t),$$
$$B_2(t) - B_2(0) = B_{2n}(t) - G_{6n}(t),$$
$$N_2(t) - N_2(0) = N_{2n}(t) - G_{7n}(t),$$
$$M(t) - M(0) = M_n(t) - G_{8n}(t),$$
$$T(t) - T(0) = T_n(t) - G_{9n}(t),$$
$$R(t) - R(0) = R_n(t) - G_{10n}(t).$$

By incorporating triangular inequality property and Lipschitz condition of X_1, we construct the following:

$$\begin{aligned} ||G_{1n}(t)|| &= ||\frac{\zeta^{1-\alpha}}{\Gamma(\alpha)}\int_0^t [X_1(\vartheta, S) - X_1(\vartheta, S_{n-1})]d\vartheta|| \\ &\leq \frac{\zeta^{1-\alpha}}{\Gamma(\alpha)}\int_0^t |||[X_1(\vartheta, S) - X_1(\vartheta, S_{n-1})]|||d\vartheta \\ &\leq \frac{\zeta^{1-\alpha}}{\Gamma(\alpha)}\Upsilon_1 ||S - S_{n-1}||t. \end{aligned}$$

By repeating the above steps in a recursive manner we get

$$||G_{1n}(t)|| \leq [\frac{\zeta^{1-\alpha}}{\Gamma(\alpha)}t]^{n+1}{\Upsilon_1}^{n+1}\Theta_1.$$

At t^*, we get

$$||G_{1n}(t)|| \leq [\frac{\zeta^{1-\alpha}}{\Gamma(\alpha)}t^*]^{n+1}{\Upsilon_1}^{n+1}\Theta_1.$$

Taking limit on the above equation as $n \to \infty$, we get

$$\lim_{n\to\infty} ||G_{1n}(t)|| \leq \lim_{n\to\infty} [\frac{\zeta^{1-\alpha}}{\Gamma(\alpha)} t^*]^{n+1} {\Upsilon_1}^{n+1} \Theta_1.$$

By using the hypothesis, $\frac{\zeta^{1-\alpha}}{\Gamma(\alpha)} t^* \Upsilon_i < 1$, we conclude that $||G_{1n}(t)|| \to 0$.
In a similar sense, we can conclude that, $||G_{in}(t)|| \to 0,\ i = 2,3,\cdots,10$. Thus there exists at least one solution of the system. □

Theorem 3. *If the condition* $(1 - \frac{\zeta^{1-\alpha}}{\Gamma(\alpha)} t)\Upsilon_i > 0$, *for* $i = 1,2,\cdots,10$ *hold, then system (6) has a unique solution.*

Proof. Let us consider $S^*(t), {C_1}^*(t), {B_1}^*(t), {N_1}^*(t), {C_2}^*(t), {B_2}^*(t), {N_2}^*(t), M^*(t), T^*(t)$ and $R^*(t)$ be another solution of the system (6), then

$$\begin{aligned} ||S(t) - S^*(t)|| &= \frac{\zeta^{1-\alpha}}{\Gamma(\alpha)} \int_0^t [X_1(\vartheta, S) - X_1(\vartheta, S^*)] d\vartheta \\ &\leq \frac{\zeta^{1-\alpha}\Upsilon_1}{\Gamma(\alpha)} t ||(S)(t) - (S^*)(t)||. \end{aligned}$$

Substituting the assumed hypothesis we obtain, $(1 - \frac{\zeta^{1-\alpha}\Upsilon_1}{\Gamma(\alpha)} t)||S(t) - S^*(t)|| \leq 0$. This implies further that, $||S(t) - S^*(t)|| > 0$. Then $S(t) = S^*(t)$. By following the same process to each solution for $i = 2,3,\cdots,10$ we get $C_1(t) = {C_1}^*(t),\ B_1(t) = {B_1}^*(t),\ N_1(t) = {N_1}^*(t),\ C_2(t) = {C_2}^*(t),\ B_2(t) = {B_2}^*(t),\ N_2(t) = {N_2}^*(t),\ M(t) = M^*(t),\ T(t) = T^*(t)$ and $R(t) = R^*(t)$.
Hence the theorem is proved. □

4 Numerical simulations

This section provides the numerical solution for the fractional-order system (6). This system of ODEs are solved using Euler's method. Further consider three cases where the system is derived for fractional order $\alpha = 0.3$, $\alpha = 0.5$ and $\alpha = 0.8$ where each equation governs evolution of states: S, C_1, B_1, N_1, C_2, B_2, N_2, M, T and R. The fractional order α in the model characterizes the strength of memory and hereditary properties present in the cardiac tissues. Physically, the smaller the fractional order is for example, $\alpha = 0.3$, the stronger the memory effects, which capture long-lasting cellular response and delayed recovery processes after ischemic stress or inflammation. In contrast, larger values, for example, $\alpha = 0.8$, reflect weaker memory and thus approach the classical integer-order dynamics where the system is at any instant determined predominantly by instantaneous interactions. Therefore, depending on α, the model effectively characterizes the degree of viscoelasticity, diffusion, and long-term dependency in myocardial tissues and allows one to gain insight into how past physiological states can influence the present development of infarction.

Let the system of equation (5) with fractional order α and including its corresponding parameters

and initial conditions are given as:

$$\begin{aligned}
\frac{d^{\alpha}S(t)}{dt^{\alpha}} &= 0.9-(0.03+0.04+0.02+0.002)S(t)\\
&= 0.9-0.092S(t),\ S(0)=0.15,\\
\frac{d^{\alpha}C_1(t)}{dt^{\alpha}} &= 0.03S(t)-(0.03-0.45-0.002)C_1(t)\\
&= 0.03S(t)+0.422C_1(t),\ C_1(0)=0.10,\\
\frac{d^{\alpha}B_1(t)}{dt^{\alpha}} &= 0.04S(t)+0.45C_1(t)+0.3N_1(t)-(0.04+0.002)B_1(t)\\
&= 0.04S(t)+0.45C_1(t)+0.3N_1(t)-0.042B_1(t),\ B_1(0)=0.10,\\
\frac{d^{\alpha}N_1(t)}{dt^{\alpha}} &= 0.02S(t)-(0.3+0.05+0.002)N_1(t)\\
&= 0.02S(t)-0.352N_1(t),\ N_1(0)=0.8,\\
\frac{d^{\alpha}C_2(t)}{dt^{\alpha}} &= 0.03C_1(t)-(0.04+0.007+0.002)C_2(t)\\
&= 0.03C_1(t)-0.049C_2(t),\ C_2(0)=0.7,\\
\frac{d^{\alpha}B_2(t)}{dt^{\alpha}} &= 0.04B_1(t)-(0.02+0.005+0.002)B_2(t)\\
&= 0.04B_1(t)-0.027B_2(t),\ B_2(0)=0.6,\\
\frac{d^{\alpha}N_2(t)}{dt^{\alpha}} &= 0.05N_1(t)-(0.05+0.003+0.002)N_2(t)\\
&= 0.05N_1(t)-0.055N_2(t),\ N_2(0)=0.5,\\
\frac{d^{\alpha}M(t)}{dt^{\alpha}} &= 0.04C_2(t)+0.02B_2(t)+0.05N_2(t)-(0.009+0.09+0.002)M(t)\\
&= 0.04C_2(t)+0.02B_2(t)+0.05N_2(t)-0.101M(t),\ M(0)=0.5,\\
\frac{d^{\alpha}T(t)}{dt^{\alpha}} &= 0.007C_2(t)+0.009M(t)+0.005B_2(t)+0.003N_2(t)-(0.3+0.09+0.002)T(t)\\
&= 0.007C_2(t)+0.009M(t)+0.005B_2(t)+0.003N_2(t)-0.392T(t),\ T(0)=0.5,\\
\frac{d^{\alpha}R(t)}{dt^{\alpha}} &= 0.3T(t)-0.002R(t),\ R(0)=0.5.
\end{aligned}$$

The graphical results obtained from the numerical simulation of the ten state variables are illustrated in Figures 2 and 3.

5 Computational methodology

The methodology utilized in this study was well-designed to explore the dynamics of a system using a combination of numerical simulation methods and predictive modeling with machine learning. A two-stage computational model was used, starting from the numerical solution of the governing fractional -order differential equations, and subsequent neural network-based modeling of the simulated outcomes.

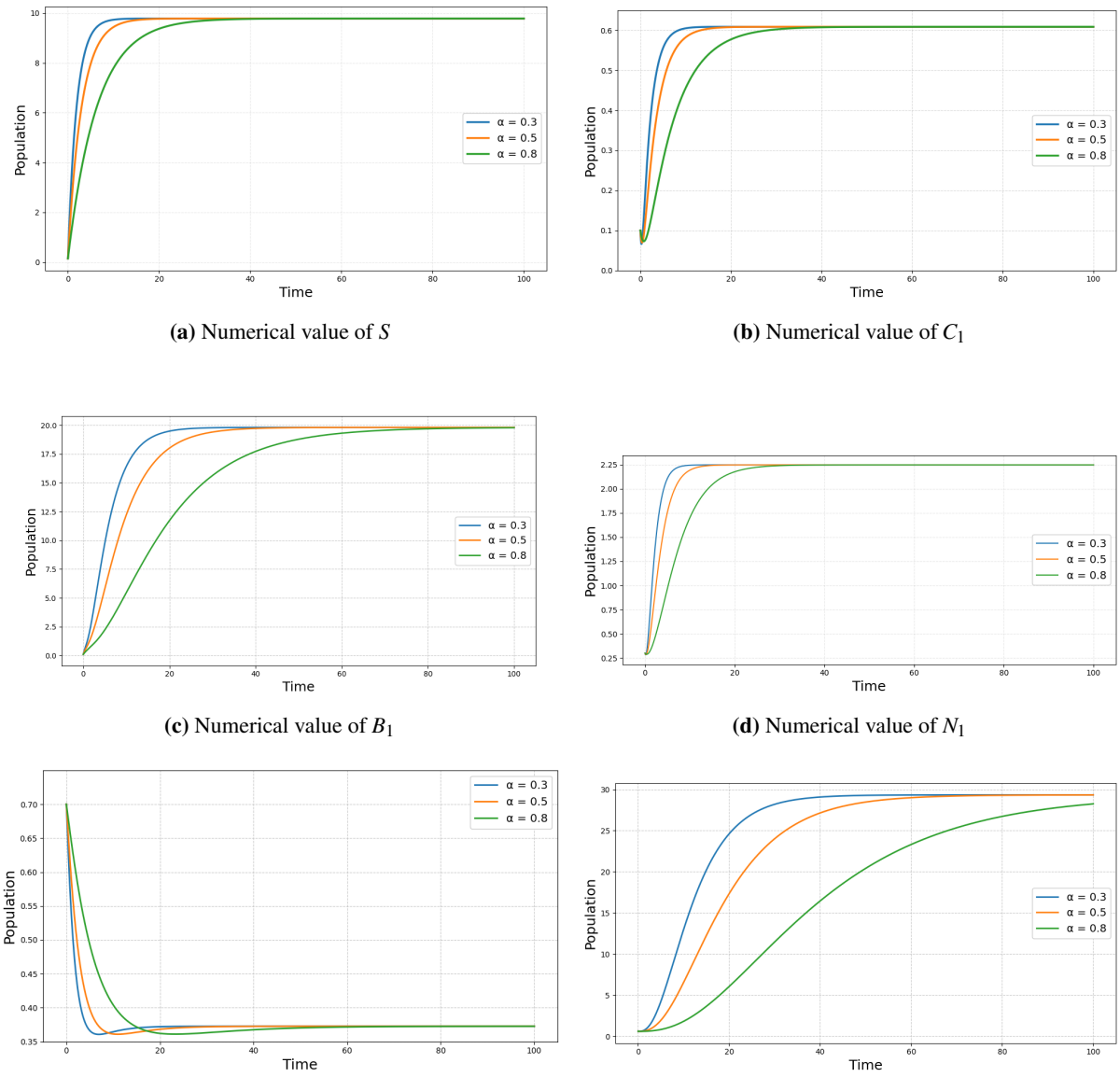

(a) Numerical value of S

(b) Numerical value of C_1

(c) Numerical value of B_1

(d) Numerical value of N_1

(e) Numerical value of C_2

(f) Numerical value of B_2

Figure 2: Comparison results of numerical simulation for compartments S, C_1, B_1, N_1, C_2, B_2 with three different fractional orders

The use of this hybrid methodology allowed for both theoretical examination and data-driven predictions of the system behavior for different memory effects.

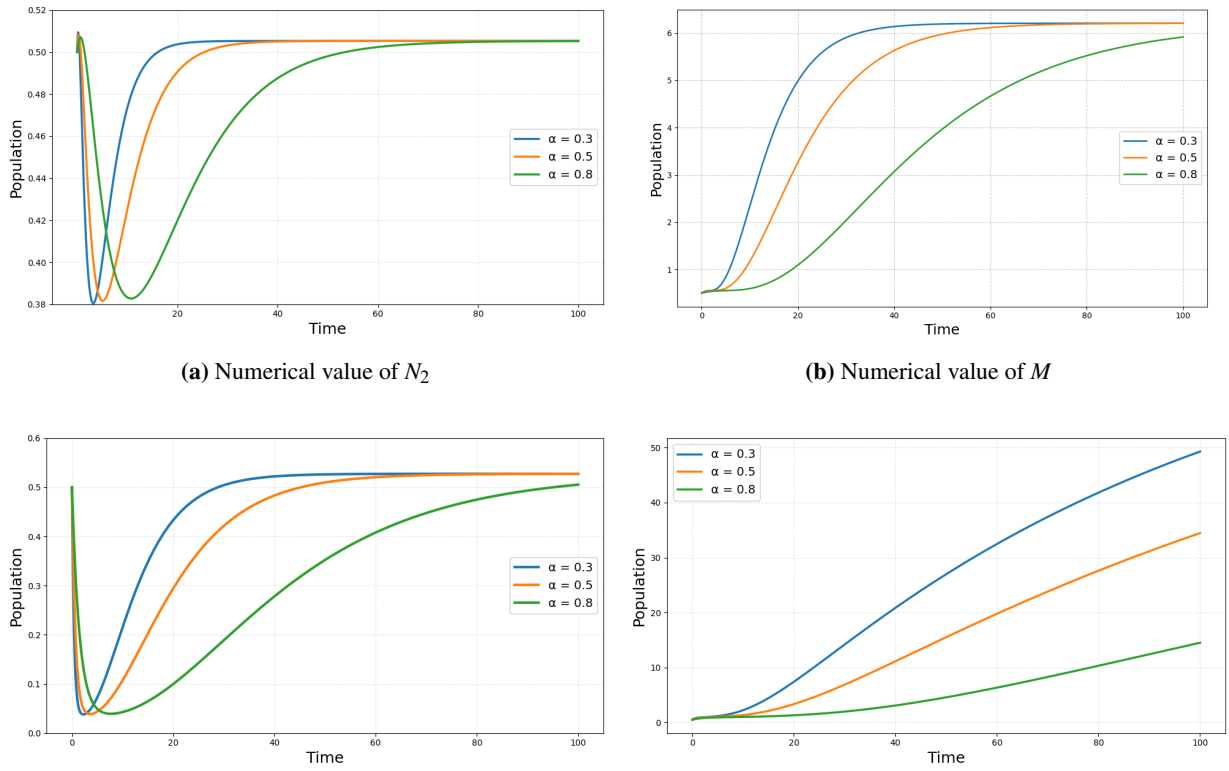

(a) Numerical value of N_2

(b) Numerical value of M

(c) Numerical value of T

(d) Numerical value of R

Figure 3: Comparison results of numerical simulation for compartments N_2, M, T, R with three different fractional orders

The results obtained through numerical method are simulated for a duration of 200 days using Adams–Bashforth–Moulton predictor–corrector method since it provides a balance between computational efficiency and stability in fractional-order systems. Iterative correction at each time step size of $h = 0.1$ days was done using the *fsolve* function with a tolerance of 10^{-6} in every integration time step, which gives convergence in every step. Therefore, the local truncation error of this method is of order $\mathcal{O}(h^{1+\alpha})$, which confirms that the numerical solution converges to the exact solution as $h \to 0$. The stability and convergence of this predictor–corrector method are checked based on the simulation parameters. The time-series output of ten state variables $(S, C_1, B_1, N_1, C_2, B_2, N_2, M, T, R)$ generated through this approach becomes the dataset for the next stage of neural network architecture.

The second step involved the creation of a Bayesian Regularized Neural Network (BRNN) using MATLAB to forecast the dynamics of the system. The architecture of the neural network was created in such a way as to comprehend the intricacy of the input–output relationship without creating redundant computational load. The basic structure of the neural network comprises of an input layer, intermediary hidden layers and lastly an output layer. A simple representation of the interconnected layers is shown in Figure 4. The input layer consists a single neuron that covered the time variable represented in days. Two hidden layers were incorporated, both with 32 and then 16 neurons, utilizing log-sigmoid activation functions because of their smooth, differentiable nature and capacity to model nonlinear relationships

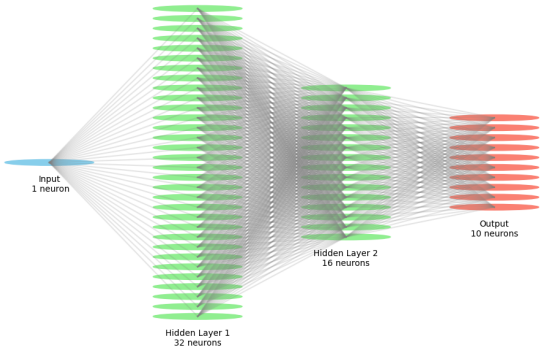

Figure 4: Artificial neural network architecture representing the layers and neurons

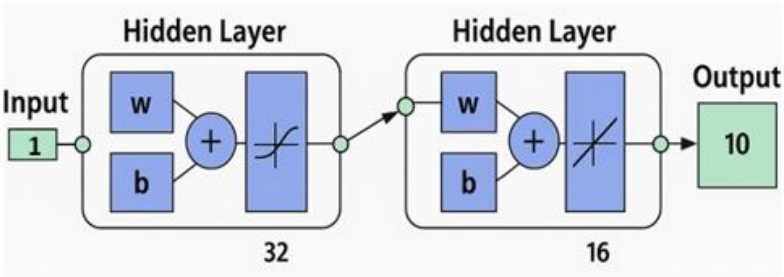

Figure 5: Schematic diagram of neural network diagram

using their signature S-shaped response curves.

The output layer consists of ten neurons uses linear activation function to predict the ten compartments of the mathematical model for direct simultaneous prediction of all system variables. Before training, all input data were screened under min–max normalization technique to normalize features into the range $[0, 1]$ so that uniform weighting is assured in learning and numerical domination by high magnitude variables is avoided. Figure 5 depicts a schematic view of the fully connected BRNN.

The dataset was divided into three subsets with 70% for training, 15% for validation, and 15% for testing. This division scheme guaranteed adequate data for learning while allowing independent samples for objective measurement of generalization performance.

Training was performed with hyperparameters optimized, having up to 500 epochs to ensure enough learning without too much computation, and a learning rate of 0.001 to facilitate stable convergence without oscillations. The division function applied is *divideind*, performance function = RMSE, and error tolerance $= 10^{-8}$. To make the results more reproducible a fixed random seed ($\texttt{rng}(0)$) was incorporated.

Root Mean Square Error (RMSE) was selected as the loss function using (*trainbr*) as the training algorithm because it is sensitive to major differences and has a direct interpretation in relation to the physical system being investigated. Such a Bayesian regularization paradigm provided an automated tradeoff between model complexity and training error by incorporating prior distributions into network parameters and performing evidence maximization. These procedures not only avoided overfitting but also yielded, in general, predictions from the network uncertainty estimates that improved interpretability

as well as reliability. The combination of both fractional-order numerical simulation and Bayesian – regularized neural network modeling resulted in a stable and precise framework for the analysis and prediction of the system behaviors under various memory-dependent situations.

6 Results and discussions

Case 1: The RMSE plot of analysis in Figure 6a illustrates the RMSE range for training, validation, and testing versus epochs, revealing a consistent decrease with the best validation performance (7.697×10^{-9}) at epoch 92. Figure 6b illustrates several subplots monitoring training parameters at epoch 92, such as a very low gradient value of 4.1048×10^{-5} illustrating few weight updates and a moderate damping parameter $\mu = 50$ providing damped optimization. The training in Case 1 converged well with extremely low RMSE and gradient values, indicating that the network optimized extremely well by epoch 92 without overfitting, as evidenced by consistent validation performance. Case 1 prediction error histogram Figure 7a indicates errors are predominantly focused approximately at 6.12×10^{-8} for training, validation, and test datasets, showing very small deviations from targets. Regression analysis in Figure 7b verifies the perfect correlation ($R = 1$) for all datasets with slopes equal to 1 and predictions coincide almost exactly on the $Y = T$ line. These outcomes demonstrate virtually flawless model precision and outstanding generalization.

Case 2: The RMSE plot of analysis of Figure 6c shows the RMSE range for training, validation, and testing across epochs, showing a steady decline with the best validation performance (6.2463×10^{-9}) achieved at epoch 41. Figure 6d presents enumerous subplots tracking training parameters at epoch 87, including a minimal gradient value of 2.1105×10^{-5}, indicating infrequent weight updates, and a damping parameter $\mu = 50$ suggesting controlled optimization. The training in Case 2 converged effectively, with low RMSE and gradient values, illustrating that the network is optimized efficiently by epoch 87 without signs of overfitting, as supported by stable validation performance. The prediction error histogram Figure 7c for Case 2 indicates prediction errors primarily bunched between roughly -2.4×10^{-5} and 2.03×10^{-5} for training, validation, and test sets, demonstrating very small deviations from the target. The regression analysis in Figure 7d verifies perfect correlation ($R = 1$) in all datasets, which denote that predictions are almost identical to the $Y = T$ line. These findings are indicative of near-perfect model precision and generalization.

Case 3: The RMSE analysis shown in Figure 6e, highlights the range of RMSE values for training, validation, and testing across epochs, showing a consistent decreased trend with optimal validation performance (4.0239×10^{-8}) achieved at epoch 69. The training state plots in Figure 6f unravel key optimization metrics at this epoch, including a minimal gradient value of 1.0388×10^{-5} suggesting stable convergence, and an adaptive damping parameter $\mu = 69$ indicating well-balanced optimization. The training process in Case 3 exhibited excellent convergence characteristics, with both RMSE and gradient values reaching very low levels by epoch 69. The simultaneous improvement in training and validation metrics confirms effective learning is possible without overfitting of the model. The histogram Figure 8a of prediction error for Case 3 indicates that errors are mostly bunched between approximately -5.4×10^{-5} and 2.08×10^{-5} for training, validation, and test sets, corresponding to very small deviations from the targets. The regression analysis shown in Figure 8b indicates perfect correlation ($R = 1$) across all datasets, with slopes of 1 and showing that predictions are nearly on the $Y = T$ line exactly.

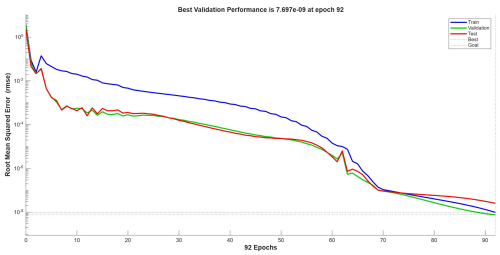

(a) RMSE analysis for Case 1

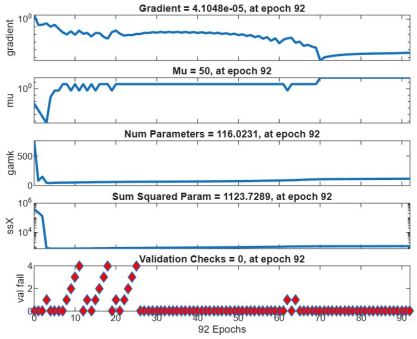

(b) Model learning state for Case 1

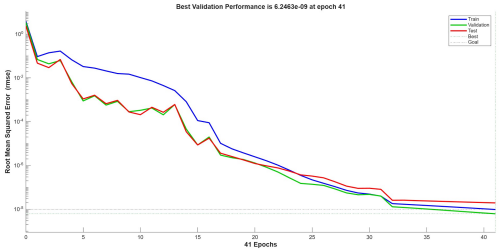

(c) RMSE analysis for Case 2

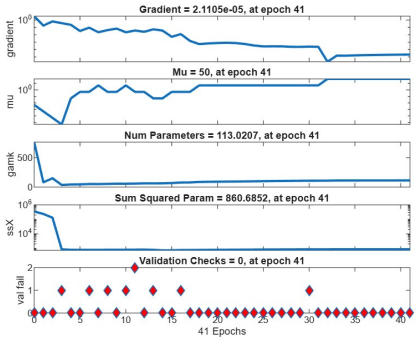

(d) Model learning state for Case 2

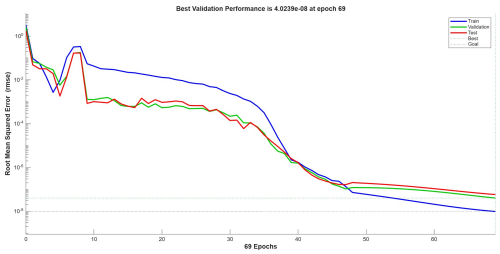

(e) RMSE analysis for Case 3

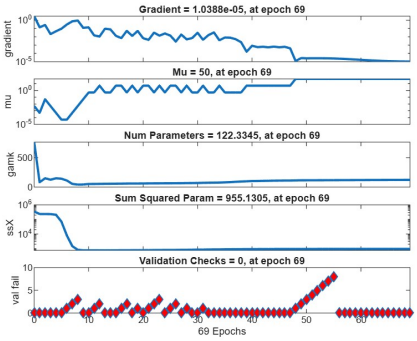

(f) Model learning state for Case 3

Figure 6: Training plots showing RMSE and model learning progression

These findings demonstrate perfect model accuracy and excellent generalization.

7 Sensitivity analysis

Sensitivity analysis has been performed to analyze the influence of variations in the fractional order α on the predictive behavior of the myocardial infarction model. The fractional order represents the

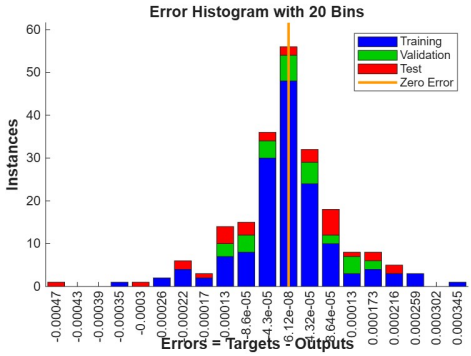

(a) Error distribution for Case 1

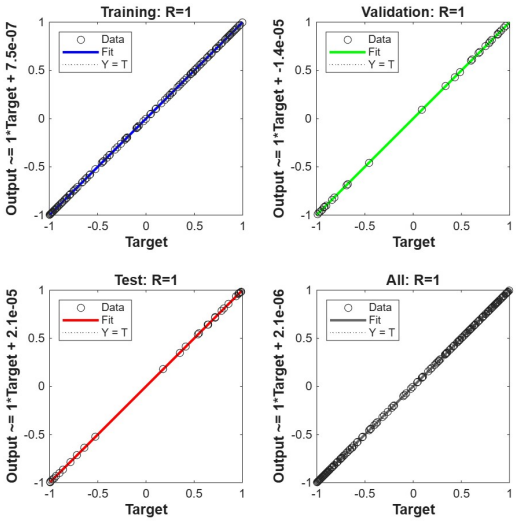

(b) Regression analysis for Case 1

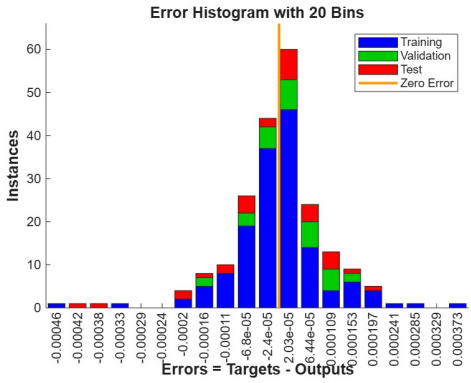

(c) Error distribution for Case 2

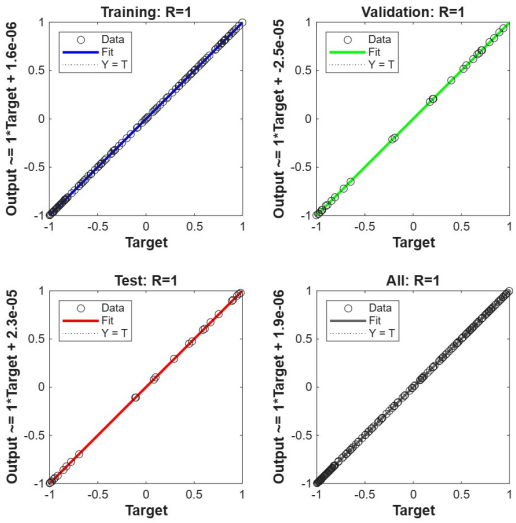

(d) Regression analysis for Case 2

Figure 7: Performance plots representing error distribution and regression study for Case 1 and Case 2

degree of memory embedded in the system. A smaller value of α reflects stronger memory effects, while with higher values, the dynamics approach the classical integer–order case. We vary α through 0.0, 0.3, 0.5, 0.8, and 1.0 to analyze the time response of the model and its deviation at steady state. The results obtained show that the system is highly sensitive for the variation of the fractional-order parameter; smaller values of α provide slower recoveries due to stronger memory effects, while higher values of α provide fast convergence toward equilibrium. Such behavior underlines the importance of α in modeling realistic myocardial recoveries and thus in the validation of the fractional-order repre-

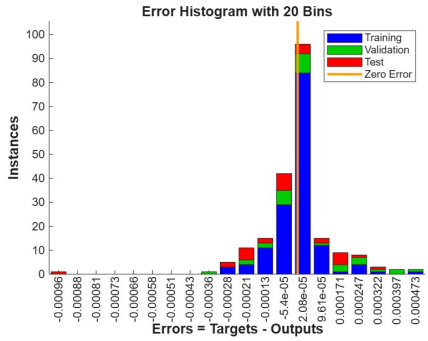

(a) Error distribution for Case 3

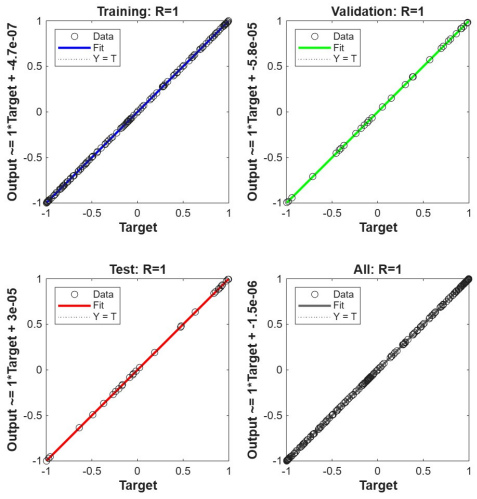

(b) Regression analysis for Case 3

Figure 8: Performance plots representing error distribution and regression study for Case 3

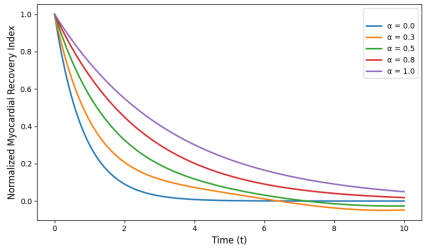

Figure 9: Sensitivity analysis of MI recovery

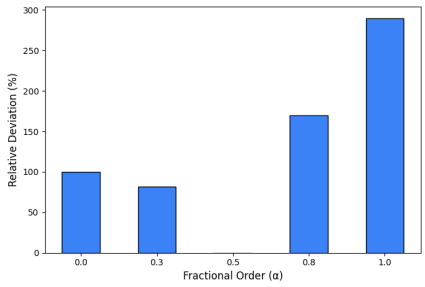

Figure 10: Sensitivity analysis across various fractional orders

sentation of cardiac tissue memory. Figure 9 Time-dependent sensitivity of myocardial recovery for different fractional orders (α). It can be seen that by increasing α, the normalized myocardial recovery index converges more rapidly, which means faster recovery dynamics. Figure 10 Relative deviation of model predictions across fractional orders. The bar graph quantifies the steady-state deviations relative to

$\alpha = 0.5$, showing that sensitivity increases with increasing α, underlining the influence of the fractional order on model stability and recovery accuracy.

8 Conclusion

This work is an attempt to develop a novel fractional-order ten compartmental model to analyze myocardial infarction (MI) dynamics in females, with emphasis on the combined effects of combined oral contraceptive pill (COCP) consumption and comorbidities like hypertension, diabetes, hypercholesterol, and more. The mathematical model uses Caputo fractional derivatives to account for memory effects and simulates disease progression by ten interacting compartments. Numerical solutions for three fractional orders ($\alpha = 0.3, 0.5, 0.8$) were simulated for a period of 200 days by using the Adams–Bashforth–Moulton Predictor–Corrector method, and simulated outputs were utilized for training a Bayesian Regularized Neural Network (BRNN) for predictive modeling. The BRNN obtained very low best validation RMSE values of 7.697×10^{-9} for Case 1, 6.2463×10^{-9} for Case 2, and 4.0239×10^{-8} for Case 3, as well as very low magnitude of gradients and ideal correlation ($R = 1$) for all datasets. Prediction error histograms reveal errors tightly bunched near zero, and regression plots verify predicted outputs follow almost exactly target values for all ten compartments. On the basis of RMSE values and performance plots, the neural network model obtains practically perfect reconstruction of simulated MI dynamics with minimal departure from true values, establishing its ability to generalize correctly and act as a strong predictive tool for interpreting MI risk development in women.

Conflicts of interest

The authors declare that there are no conflicts of interest.

References

[1] C.E. Agbo, R.T. Abah, A.M. Abdullahi, *A mathematical modeling on the stability analysis of heart disease dynamics*, J. Inst. Res. Big Data Anal. Innov. **2(2)** (2024) 165—171.

[2] C.E. Agbo, R.T. Abah, F.O. Ogunfiditimi, *Mathematical modeling and stability analysis of the disease-free equilibrium of heart disease transmission and prevention dynamics*, Fac. Nat. Appl. Sci. J. Math. Model. Numer. Simul. **2** (2025) 165–171.

[3] B. Chen-Charpentier, H. Kojouharov, *Sensitivity analysis and uncertainty of a myocardial infarction model*, Mathematics, **12** (2024) 2217.

[4] P. Croft, P.C. Hannaford, *Risk factors for acute myocardial infarction in women: evidence from the Royal College of General Practitioners' oral contraception study,* BMJ **298** (1989) 165–168.

[5] K. Diethelm, *The analysis of fractional differential equations: An application-oriented exposition using operators of Caputo type*. Lect. Notes Math. 2004.

[6] Y. Fang, Y. Wu, L. Gao, *Machine learning-based myocardial infarction bibliometric analysis*, Front. Med. **12** (2025) 1477351.

[7] A. Gompel, G. Plu-Bureau, N. Lahlou, F. Couturaud, S. Uhry, E. Blicq, C. Mounier-Vehier, A. Bellemain-Appaix, E. Vautrin, C.B.D. Sollier, L. Drouet, *Contraception and risk factors in young women with myocardial infarction: The WAMIF study*, Eur. J. Obstet. Gynecol. Reprod. Biol. **313** (2025) 114568.

[8] G. Grigorian, S.V. George, S. Lishak, R.J. Shipley, S. Arridge, *A hybrid neural ordinary differential equation model of the cardiovascular system*, J. R. Soc. Interface, **21** (2024) 20230710.

[9] M. Hammad, M.H. Alkinani, B.B. Gupta, A.A. Abd El-Latif, *Myocardial infarction detection based on deep neural network on imbalanced data*, Multimed. Syst. **28** (2022) 1373–1385.

[10] A.A. Hamou, E. Azroul, Z. Hammouch, A.L. Alaoui, *A fractional multi-order model to predict the COVID-19 outbreak in Morocco*, Appl. Comput. Math, **20(1)** (2020) 177–203.

[11] A.A. Hamou, R.R. Rasul, Z. Hammouch, N. Özdemir, *Analysis and dynamics of a mathematical model to predict unreported cases of COVID-19 epidemic in Morocco*, Appl. Comput. Math. **41(6)** (2022) 289.

[12] S.S.S. Banu, T. Gunasekar, P. Raghavendran, S.S. Santra, D. Baleanu, *Mathematical and Computational Modeling of IVF: Predicting Success with Artificial Neural Network*, Adv. Math. Models Appl. **10(3)** (2025) 429–449.

[13] S. Haykin, *Neural Networks and Learning Machines*, 3rd edition Pearson Education India, 2009.

[14] Ø. Lidegaard, E. Løkkegaard, A. Jensen, C.W. Skovlund, N. Keiding, *Thrombotic stroke and myocardial infarction with hormonal contraception*, N. Engl. J. Med. **366** (2012) 2257–2266.

[15] N. Madani, E.H. Azroul, Z. Hammouch, *New model of HIV/AIDS dynamics based on Caputo–Fabrizio derivative order: Optimal strategies to control the spread*, J. Comput. Sci. (2025) 102612.

[16] N. Madani, Z. Hammouch, N. Ozdemir, *Hybrid GA-IPA and neural network-based solution for fractional-order nonlinear predator–prey dynamical systems*, Nonlinear Dyn. (2025) 1–26.

[17] Z.A. Noor, I. Talib, M.B. Riaz, *Computational advancements in spectral methods for solving fractional-order differential equations*, Fractals, **33(6)** (2025) 1–17.

[18] L.R. Pedersen, D. Frestad, M.M. Michelsen, N.D. Mygind, H. Rasmusen, H.E. Suhrs, E. Prescott, *Risk factors for myocardial infarction in women and men: a review of the current literature*, Curr. Pharm. Des. **22** (2016) 3835–3852.

[19] S. Rashid, Z. Hammouch, D. Baleanu, Y.M. Chu, *New generalizations in the sense of the weighted non-singular fractional integral operator*, Fractals **28(8)** (2020) 2040003.

[20] S.G. Samko, A.A. Kilbas, O.I. Marichev, *Fractional Integrals and Derivatives: Theory and Applications*, Gordon and Breach Science Publishers, 1993.

[21] I.R. Serikkalievna, A.G. Sailaubekuly, Y.Y. Yessentaykyzy, K.A. Zhambulkyzy, B. Aida, *Myocardial infarction in young people: a modern view of pathology*, in Proc. 4th Int. Sci. Pract. Conf., Development of Higher Education: Trends and Prospects, Rotterdam, Netherlands, 28–31 Jan. Int. Sci. Group (2025) 104.

[22] S.S. Sumaiya Banu, T. Gunasekar, S. Manikandan, K. Kumar, M. Suba, *Analyzing SEITR tuberculosis transmission model using Caputo–Fabrizio fractional derivative with diverse contact rates*, Appl. Appl. Math. **20(4)** (2025) Art. 8.

[23] I. Talib, T. Abdeljawad, M.A. Alqudah, *A high-precision spectral method for solving Bagley–Torvik equations*, Comput. Appl. Math. **44** (2025) 412.

[24] B.C. Tanis, M.A. Van Den Bosch, J.M. Kemmeren, V.M. Cats, F.M. Helmerhorst, A. Algra, Y. Van Der Graaf, F.R. Rosendaal, *Oral contraceptives and the risk of myocardial infarction*, N. Engl. J. Med. **345** (2001) 1787–1793.

[25] S. Tee, A.A.M. Daud, *Mathematical model and analysis of population dynamics for heart failure and heart transplant*, J. Qual. Meas. Anal. **21** (2025) 69–85.

[26] M.P. Than, J.W. Pickering, Y. Sandoval, A.S. Shah, A. Tsanas, F.S. Apple, S. Blankenberg, L. Cullen, C. Mueller, J.T. Neumann, R. Twerenbold, *Machine learning to predict the likelihood of acute myocardial infarction*, Circulation **140** (2019) 899–909.

[27] V. Vaccarino, *Myocardial infarction in young women: an unrecognized and unexplained epidemic*, Circulation **139** (2019) 1057–1059.

[28] N. Yadav, A. Yadav, M. Kumar, *An Introduction to Neural Network Methods for Differential Equations*, Springer, 2015.

[29] H. Yonis, E. Løkkegaard, K. Kragholm, C.B. Granger, A.L. Møller, L.S. Mørch, C. Torp-Pedersen, A. Meaidi, *Stroke and myocardial infarction with contemporary hormonal contraception: real-world, nationwide, prospective cohort study*, BMJ **388** (2025)

[30] D. Zaidi, I. Talib, M.B. Riaz, M.N. Alam, *Extending spectral methods to solve time fractional-order Bloch equations using generalized Laguerre polynomials*, Part. Differ. Equ. Appl. Math. **13** (2025) 101049.

[31] M. Zamir, F. Nadeem, T. Abdeljawad, Z. Hammouch, *Threshold condition and non-pharmaceutical interventions' control strategies for elimination of COVID-19*, Results Phys. **20** (2021) 103698.

[32] D.R. Zucker, J.L. Griffith, J.R. Beshansky, H.P. Selker, *Presentations of acute myocardial infarction in men and women*, J. Gen. Intern. Med. **12** (1997) 79–87.